

# COV-ELM classifier: An Extreme Learning Machine based identification of COVID-19 using Chest X-Ray Images

Sheetal Rajpal<sup>a</sup>, Naveen Kumar<sup>a</sup>, Ankit Rajpal<sup>b,\*</sup>

<sup>a</sup>*Department of Computer Science, University of Delhi, Delhi, India*

<sup>b</sup>*Department of Computer Science, Deen Dayal Upadhyaya College, University of Delhi, Delhi, India*

---

## Abstract

Coronaviruses constitute a family of virus that particularly gives rise to respiratory diseases. Coronavirus disease (COVID-19) is an infectious disease caused by a newly discovered coronavirus also termed as Severe acute respiratory syndrome coronavirus 2 (SARS-CoV-2). Due to the rapid spread, COVID-19 outbreak has been declared a pandemic on 11th March 2020. The reverse transcription-polymerase chain reaction (RT-PCR) test is most commonly used for the qualitative assessment of the presence of SARS-CoV-2. Due to the high false-negative rate of RT-PCR test, chest X-ray (CXR) imaging has emerged to be a feasible alternative for the detection of COVID-19. In this work, we propose a multi-classification model based on extreme learning machine, COV-ELM, that aims to classify the CXR images belonging to three classes, namely COVID-19, normal, and pneumonia. The choice of ELM in this work is based on the fact that ELM significantly shortens the training time with the least interventions required to tune the networks as compared to conventional gradient-based learning algorithms. The proposed work is experimented on the COVID-19 chest X-ray (CXR) image data collected from three publicly available sources. The image data is preprocessed and local features are extracted by exploiting the frequency and texture regions to generate a feature pool. This pool of features is provided as an input to the ELM and a 10-fold cross-validation method is employed to evaluate the proposed model. The COV-ELM achieved a macro average of f1-score is 0.95 and the overall sensitivity of the COV-ELM is  $0.94 \pm 0.03$  at 95% confidence interval. The COV-ELM outperforms other competitive machine learning algorithms in a three-class classification scenario. The results of COV-ELM are quite promising which increases its suitability to be applied to bigger and more diverse datasets.

*Keywords:* COVID-19, Extreme Learning Machine, chest X-rays, Pneumonia viral, Pneumonia bacterial.

---

## 1. Introduction

Coronavirus disease 2019 (COVID-19) is a contagious infection resulting in respiratory illness in most of the cases, known to originate from Wuhan City, Hubei Province, China. COVID-19 is caused by a novel coronavirus, widely recognized as severe acute respiratory syndrome coronavirus 2 (SARS-CoV-2; previously

---

\*Corresponding author

Email addresses: [sheetal.rajpal.09@gmail.com](mailto:sheetal.rajpal.09@gmail.com) (Sheetal Rajpal), [nkumar@cs.du.ac.in](mailto:nkumar@cs.du.ac.in) (Naveen Kumar), [ankit.cs.du@gmail.com](mailto:ankit.cs.du@gmail.com) (Ankit Rajpal)

known as 2019-nCoV) [1]. Initially, it was first reported to the WHO on December 31, 2019, and later on January 30, 2020, the COVID-19 outbreak has become a global health emergency. On March 11, 2020, the WHO proclaimed COVID-19 a global pandemic [2].

The Reverse transcription-polymerase chain reaction (RT-PCR) test is the most widely used benchmark method to detect Severe acute respiratory syndrome coronavirus 2 (SARS-CoV-2). A major concern with the RT-PCR test is the likelihood of drawing out false-negative and false-positive results. It has been reported that many symptomatic cases showing characteristics of COVID-19 were not diagnosed [3] by RT-PCR test. Due to the high false-negative rate of RT-PCR test which is up to 67%, it is supplemented with other means of monitoring the clinical features of a subject.

Chest X-ray is the most common method of examining common respiratory and lung infections for fast and cost-effective diagnosis [4, 5]. Recently, several research groups have experimented on CXR images to detect COVID-19 [6, 7, 8, 9] which can rule out the chance of the doctors getting infected by the COVID-19 patients. The major challenge is the similarity between COVID-19 and pneumonia caused by other infections [10]. In this paper, the Extreme Learning Machine (ELM) classifier is used to separate out COVID-19 cases from normal and pneumonia cases.

Several research groups have recently applied some well known deep neural networks like AlexNet (also known as 'ImageNet') [11], VGGNet [12], GoogLeNet [13], ResNet [14], and the variations of these networks for the classification of COVID-19 on chest X-ray images [7, 8, 9]. ImageNet has 60 million parameters and 650,000 neurons, trained through the dataset of 1.2 million images, which took almost a week on two NVIDIA GTX 580 3GB GPUs [11]. VGGNet has 144 million parameters and greater depth compared to ImageNet but it is conjectured that it converges in fewer epochs due to regularization, smaller filter sizes, pre-initialization of certain layers [12]. GoogLeNet [13] utilizes a 22 layers deep network for 1.2 million images in training set, 50,000 in validation set, and 100,000 images in testing set. Szegedy et al. [13] used an more exhaustive cropping approach than that of Krizhevsky et al. [11]. ResNet was experimented with CIFAR-10 dataset [15] with 50k training images, 10k testing images and with 23 million trainable parameters depicting good generalization performance [14].

Khan et al. [7] proposed a deep convolutional neural network (DCNN) model to automate the detection of COVID-19 in chest X-ray images. The model is based on Xception architecture [16] pre-trained on ImageNet [11] and achieved an overall accuracy of 89.6%. T. Mahmud et al. [8] proposed a DCNN model using a variation in dilation rate to extract distinguishing features from chest X-ray images and achieved an accuracy of 90.2% for multi-class classification (COVID-19/Normal/Pneumonia). They also used Gradient-weighted Class Activation Mapping (Grad-CAM) to visualize the abnormal regions of CXR scans corresponding to different types of pneumonia. Wang et al. [9] developed a computer-aided screening for COVID-19 CXR images based on an already trained network on ImageNet tuned with the Adam optimizer and achieved 91% sensitivity for COVID-19 cases. Basu et al. [17] used domain extension transfer learning (DETL) with 12-layers by using already trained network on National Institutes of Health (NIH) CXR image dataset [4]

(comprising 108, 948 frontal view X-ray images of 32,717 unique patients) further fine-tuned for COVID-19 dataset to obtain the overall accuracy  $95.3\% \pm 0.02$  on 5-fold cross-validation. Rajaraman et al. [18] iteratively pruned the task-specific models (VGG-16, VGG-19, and Inception-V3) by pruning 2% of the neurons in each convolutional layer and retrain the model to obtain a macro average of 0.99 for f1-score.

Khuzani et al. [10] used multilayer neural networks (MLNN) to distinguish the CXR images of COVID-19 patients from other forms of pneumonia. The spatial and frequency domain features are extracted from the X-ray images. Based on the evaluation of extracted features, they conjectured that the fast fourier transform (FFT) features are the best group of features in determining the COVID-19 case and while the normal class is best determined by gray level difference method (GLDM). These features are further reduced by principal component analysis (PCA) to generate an optimized set of synthetic features and provided as an input to MLNN which distinguishes COVID-19 images with an accuracy of 94% from non-COVID-19 cases.

Training an MLNN and DCNN requires intensive computational performance and generally a time-consuming task. The research groups are mainly focused on the use of deep neural networks which requires millions of parameters and the optimal choice of hyper-parameters is very critical that impacts the overall performance. Therefore, the proposed work considered reducing this bottleneck by making use of a single hidden layer feed-forward neural network (SLFN) known as extreme learning machine (ELM) [19, 20].

The ELM is a batch learning algorithm proposed by Huang et al. [19] and has been used extensively in different domains like ECG signal classification [21] and Identification of arrhythmia disease [22]. The ELM and its variants have also been applied in other domains such as fingerprint identification [23], lung cancer detection [24], image and video watermarking [25, 26], and 3D object recognition [27]. The applications of ELM in various domains is due to its fast learning, good generalization performance, and ease of implementation. The brief review of ELM is presented in section 2. The main contribution of this paper is to explore the possibility of applying ELM on CXR images.

The rest of the paper is outlined as follows. The Section 2 presents a review of ELM, section 3 gives the dataset description followed by the detailed methodology, outcome of the experiments is discussed in section 4, followed by a detailed analysis of the results, finally the conclusions and scope of future work are discussed in section 5.

## 2. Extreme Learning Machine

Extreme Learning Machine (ELM) was proposed by Huang et al. as an efficient alternative to the backpropagation algorithm for single-layer feed-forward networks (SNFN) [19]. It is a fast learning algorithm with good generalization performance as compared to other traditional feed-forward networks. An ELM works by initializing a set of weights randomly and computing the output weights analytically by Moore Penrose Matrix Inverse [28]. Fig. 1 depicts the ELM architecture and while the algorithm 1 gives its mathematical procedure.

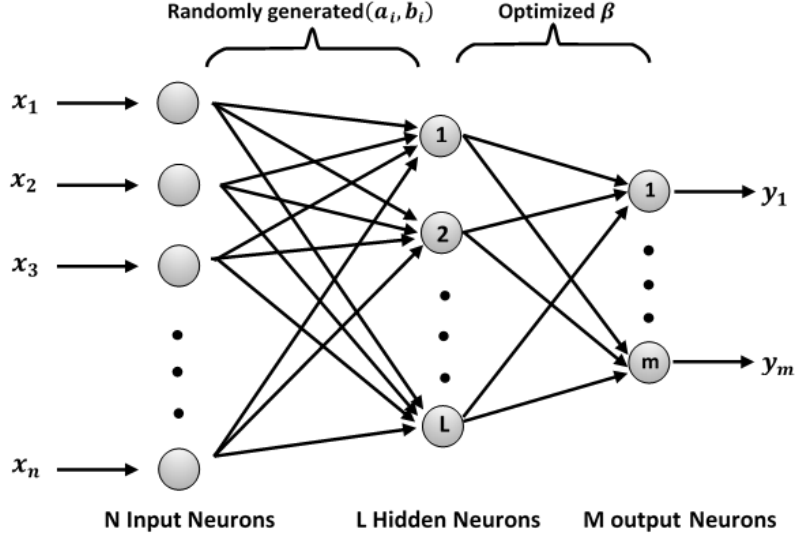


Figure 1: ELM Architecture: The ELM network comprises an input layer, a hidden layer, and an output layer

---

**Algorithm 1** ELM Algorithm

---

**Input:**

Training set:  $(x_j, t_j), x_j \in \mathbf{R}^n, t_j \in \mathbf{R}^m$  for  $j = 1, 2, \dots, N$

Activation function:  $g: \mathbf{R} \rightarrow \mathbf{R}$

Number of hidden nodes:  $L$

**Output:**

Optimized weight matrix:  $\beta$

1. Randomly assign hidden node parameters  $(a_i, b_i), i = 1, 2, \dots, L$ ;
  2. Compute the hidden-layer output matrix  $G$ ;
  3. Compute output weight vector  $\beta = G^\dagger T$
- 

Huang et al. [29] argue that ELM outperforms the conventional learning algorithms in terms of learning speed, and in most of the cases shows better generalization capability than the conventional gradient-based learning algorithms such as backpropagation where approximation the weights are adjusted with a non-linear relationship between the input and the output. They further stated that ELM can compute the desired weights of the network in a single step in comparison to classical methods.

### 3. Material and Methods

In this section, we present a list of CXR image datasets experimented in this work, followed by the preprocessing process. Subsequently, the feature extraction and the proposed architecture are briefly described.

#### 3.1. Dataset Description

In the present work, we have considered the following publicly available CXR datasets for COVID-19, Normal, and Pneumonia.

- COVID-19 Image Data Collection [6]
  - 760 samples, COVID-19: 538, ARDS: 14, Other Diseases: 222
- COVID-19 Radiography Database (Kaggle) [30]
  - 2905 samples, COVID-19: 219, Normal: 1341, Viral Pneumonia: 1345
- Mendeley Chest X-ray Images [31]
  - 5856 samples, Pneumonia (Viral and Bacterial) : 4273, Normal:1583

Since the CXR dataset is collected from different sources, we only examine the CXR with Poster anterior (PA) and Erect anteroposterior (AP) views. The first two databases in the above list comprise 520 such images. We used these images for the training purpose. We have included 520 CXR images of normal and pneumonia cases from COVID-19 Radiography Database (Kaggle) [30] and Mendeley Chest X-ray Images [31].

#### 3.2. Preprocessing

Fig. 2 depicts the preprocessing steps for the CXR image dataset, which includes resizing, normalization, and contrast limited adaptive histogram equalization (CLAHE) [32] applied in order. Due to diversity in the CXR image collection, they are resized and subjected to min-max normalization [33] to ensure uniformity. CLAHE is a variant of adaptive histogram equalization is applied further to enhance the local contrast in the CXRs.

#### 3.3. Feature Extraction

The texture is one of the significant features used in classifying images or determining the region of interest (ROI) in an image [34]. In this work, there are four group of regions are investigated to determine a set of significant features in CXR image. The first group of texture features is the statistical values (area, mean, standard deviation, skewness, kurtosis, energy, entropy, max, min, mean absolute deviation, median, range, root mean square, uniformity) directly computed from the preprocessed image of  $512 \times 512$  and placed in feature pool. Other group of texture features are extracted from the regions identified by applying gray-level

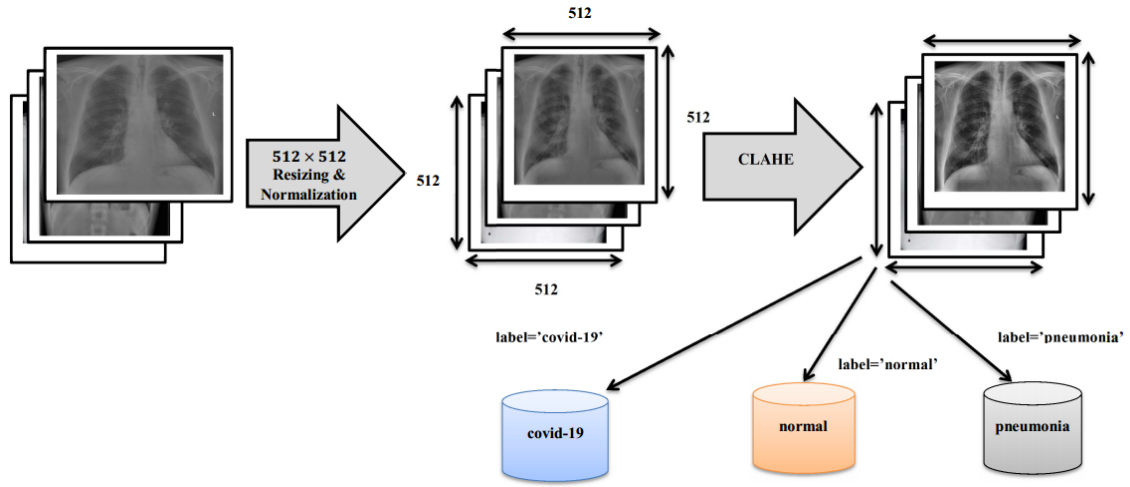


Figure 2: Preprocessing: Image Resizing, Normalization, and contrast limited adaptive histogram equalization (CLAHE).

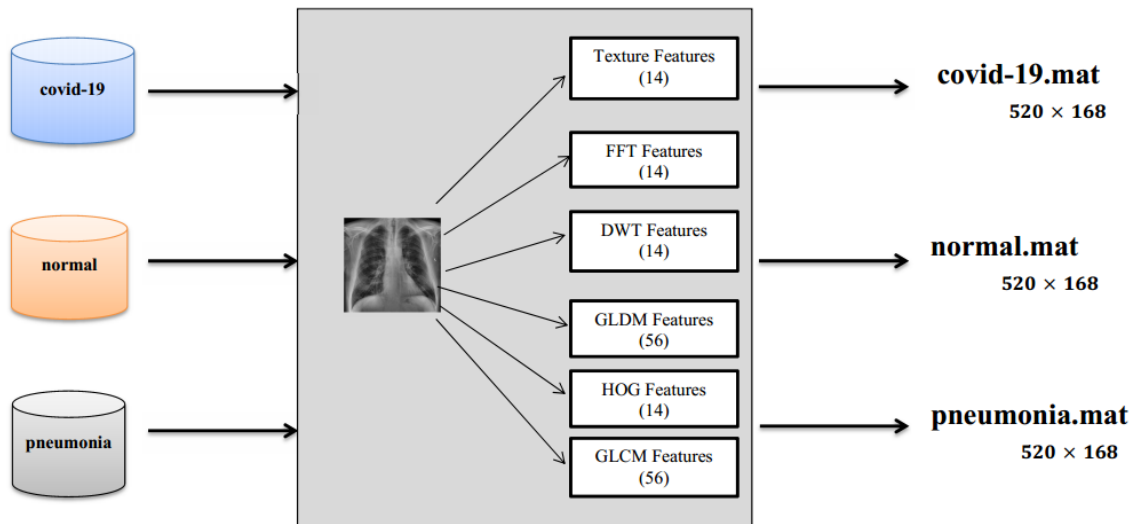


Figure 3: Feature pool generated based on Texture, FFT, DWT, DLDL, HOG, and GLDM regions.

co-occurrence matrix (GLCM) [35, 36], histogram of oriented gradients (HOG) [37, 38, 39], and gray-level difference matrix (GLDM) [40, 10]. The aforementioned statistical measures are also computed for each region - GLDM, HOG, and GLCM.

The use of frequency features is also notable in transforming an image to locate the significant regions in the medical imaging [41, 42, 43]. In the present work, the frequency features are extracted using fast fourier transform (FFT) and discrete wavelet transform (DWT). The previously mentioned statistical measures are calculated for FFT map and low-frequency (LL3) coefficients (obtained after three-level DWT) to generate a vector of frequency features. The final set of features obtained by concatenating textural feature vector of length (140) with the frequency vector of length (28) to generate a feature pool of size  $520 \times 168$  for the CXR images labeled – 'covid-19', 'normal', and 'pneumonia'. The complete process of feature extrcation is depicted in Fig. 3.

### 3.4. Evaluation of extracted features

The bar plot in Fig. 4 depicts the importance of each type of feature in the identification of COVID-19 (4(a)), Normal (4(b)), and Pneumonia (4(c)) cases. It can be seen that the FFT features are most significant in classifying the COVID-19 case, GLDM is important in determining the normal cases, and Pneumonia cases are best identified with the help of FFT, GLDM, and GLCM.

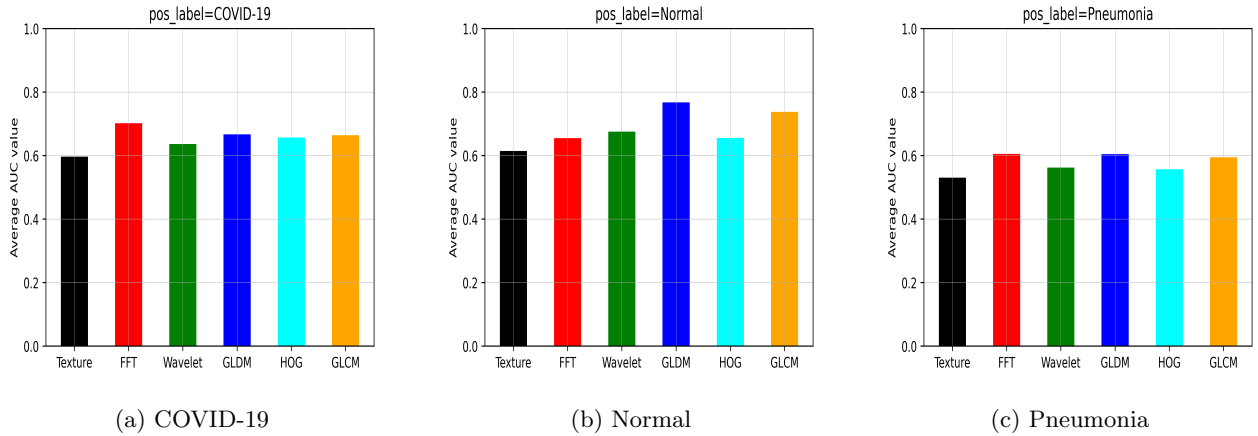


Figure 4: The bar plot showing the importance of each feature in the identification of COVID-19, Normal, and Pneumonia cases.

### 3.5. Construction of ELM Model

The feature pool of size  $1560 \times 168$  is split into training and testing set using 10-fold cross-validation 5. For each of the folds, the ELM-Train procedure is provided with 90% of the data as an input along with number of hidden neurons ( $L$ ) and activation function ( $g$ ) to generate an ELM Model. This ELM Model is used on 10% of the test data to validate the model.

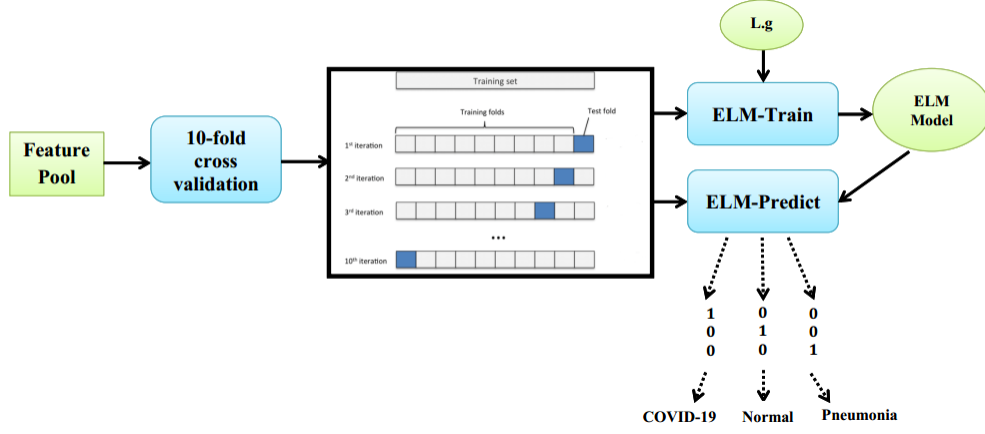


Figure 5: ELM is trained with the feature pool and 10-fold cross-validation is used to validate the model.

Figure 6 depicts the effect of increasing of the number of hidden neurons ( $L$ ) on 10-fold cross-validation accuracy. The accuracy increases with an increase in the number of hidden neurons to an extent ( $L = 350$ ) after which it shows inferior performance. It can be seen that the maximum attained accuracy under 10-fold cross-validation is 94.10% for ( $L = 350$ ).

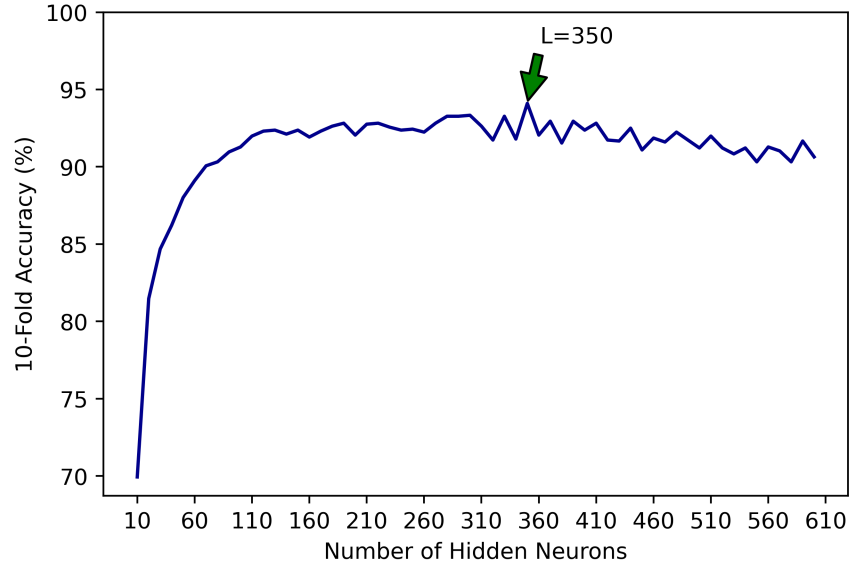


Figure 6: Effect of the increasing number of hidden neurons ( $L$ ) on 10-fold cross-validation. Accuracy increases with increasing  $L$  to an extent ( $L = 350$ ) after which it starts diminishing.

#### 4. Results and Discussion

We have carried out all the experiments using Python 3.6.9 on the NVIDIA Tesla K80 GPU. Figure 7 depicts the receiver operating characteristic (ROC) curves for each of the three classes, namely COVID-19, Normal,



and Pneumonia for one fold. It is apparent from the ROC curves that AUC is near unity for all the three classes which shows a good generalization performance of COV-ELM.

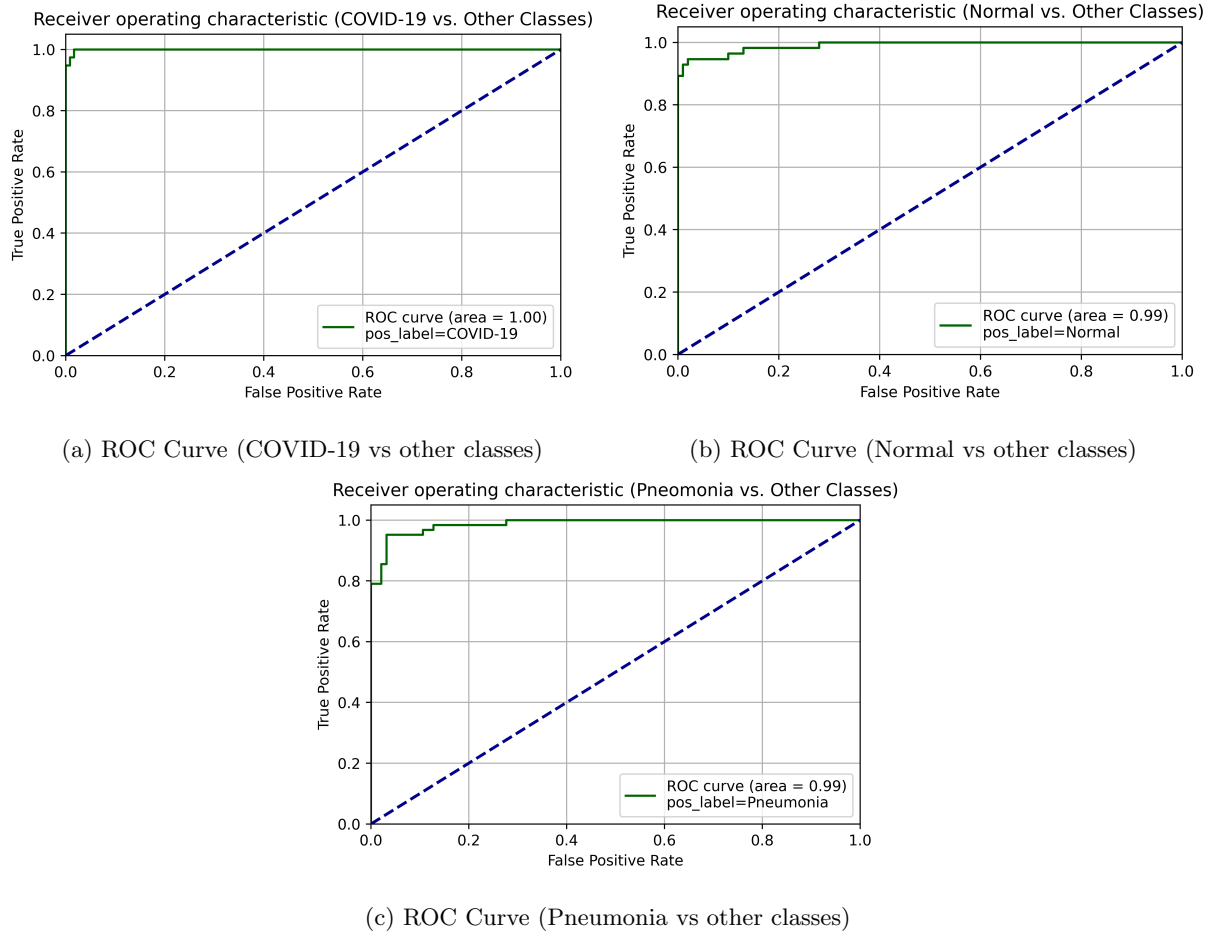


Figure 7: AUC is near unity for each of the three classes.

Fig. 8 depicts the confusion matrix and the heatmap for 10-fold cross validation. The confusion matrix (Fig. 8(a)) shows that classification error in classifying COVID-19, Normal, and Pneumonia is 3.68%, 4.46%, and 7.58% respectively and the macro average of f1-score is 0.95 as depicted in the heatmap (Fig. 8(b)).

In order to quantify the uncertainty of a classifier, the sensitivity (true positive rate / recall) value is determined at 95% confidence interval (CI) via normal approximation. In Table 1, the sensitivity value of COV-ELM in identifying COVID-19, Normal, and Pneumonia is  $0.96 \pm 0.05$ ,  $0.96 \pm 0.01$ , and  $0.92 \pm 0.03$  respectively.

Table 1: Sensitivity (Recall) values for COVID-19, Normal, and Pneumonia at 95% confidence interval.

Sensitivity at 95% CI		
COVID-19	Normal	Pneumonia
$0.96 \pm 0.05$	$0.96 \pm 0.01$	$0.92 \pm 0.03$

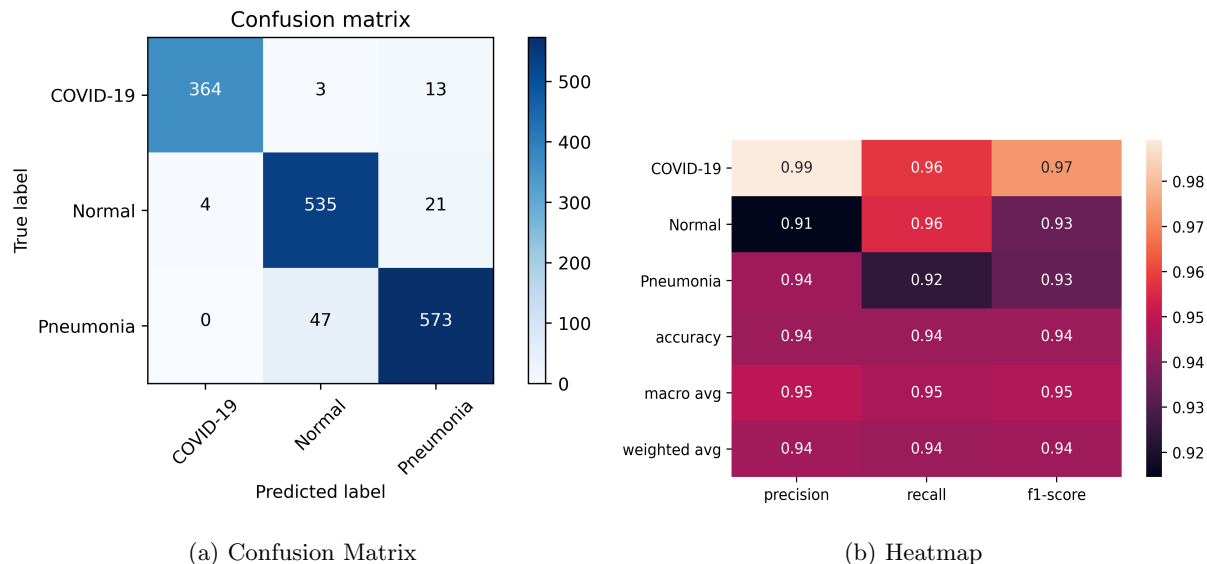


Figure 8: The classification error in classifying COVID-19, Normal, and Pneumonia is 3.68%, 4.46%, and 7.58% respectively and the macro average of f1-score is 0.95.

The COV-ELM (ELM classifier) is compared with the state-of-the-art machine learning algorithms – support vector classifier (SVC) using rbf and linear kernels, gradient boosting classifier (GBC), random forest ensemble (RBE), artificial neural networks (ANN), decision tree classifier (DTC), and voting classifier (VC) ensemble of (logistic regression (LR), SVC, and GBC). Table 2 depicts the comparative study of COV-ELM with other state-of-the-art classifiers in terms of sensitivity at 95% confidence interval (CI).

Table 2: Comparison of COV-ELM with other state-of-the-art classifiers in terms of sensitivity value at 95% confidence interval.

Classifier	Sensitivity
ELM (L=350, rbf-l2)	$0.94 \pm 0.03$
GBC (learning rate=1.0)	$0.91 \pm 0.05$
SVC (C=1.0, kernel='rbf')	$0.86 \pm 0.06$
SVC (C=1.0, kernel='linear')	$0.90 \pm 0.05$
RBE (min_samples_split=2)	$0.89 \pm 0.05$
ANN (23,747 Parameters)	$0.85 \pm 0.08$
DTC (min_samples_leaf=1)	$0.82 \pm 0.07$
VC (LR, SVC, GBC)	$0.89 \pm 0.05$

The overall sensitivity of COV-ELM is  $0.94 \pm 0.03$ , which has the minimum variance and possesses higher values as compared to other state-of-the-art classifiers.

## 5. Conclusions

Due to the lack of COVID-19 instances at one single source, the CXR image data is collected from two publicly available sources. PA and AP views of CXR are considered, preprocessed, and segregated to 'covid-19', 'normal', and 'pneumonia'. The texture features (GLDM, HOG, and GLDM) and frequency features (FFT and DWT) are extracted. It is concluded from the evaluation of extracted features that FFT features are most significant in identifying COVID-19. The number of parameters in ELM is considerably less as compared to other feed-forward neural networks requiring approx. 24,000 parameters and deep neural network which needs millions of parameters for training. The effect of an increase in the number of hidden neurons ( $L$ ) on the 10-fold cross-validation accuracy is examined and it is concluded that the accuracy increases with increasing  $L$  to an extent ( $L = 350$ ) after which it starts diminishing. The proposed method achieved a macro average of f1-score is 0.95 in a three-class classification scenario and the classification error rate 3.68% for COVID-19. The COV-ELM outperforms other competitive machine learning algorithms with the sensitivity value of  $0.94\% \pm 0.03$  at 95% confidence interval. The results of COV-ELM are quite promising which makes it suitable to apply on bigger and more diverse datasets.

## References

- [1] M.-Y. Ng, E. Y. Lee, J. Yang, F. Yang, X. Li, H. Wang, M. M.-s. Lui, C. S.-Y. Lo, B. Leung, P.-L. Khong, et al., Imaging profile of the COVID-19 infection: radiologic findings and literature review, *Radiology: Cardiothoracic Imaging* 2 (1) (2020) e200034.
- [2] WHO, Archived: WHO Timeline - COVID-19, <https://www.who.int/news-room/detail/27-04-2020-who-timeline---covid-19> (2020).
- [3] A. Tahamtan, A. Ardebili, Real-time RT-PCR in COVID-19 detection: issues affecting the results (2020).
- [4] X. Wang, Y. Peng, L. Lu, Z. Lu, M. Bagheri, R. M. Summers, Chestx-ray8: Hospital-scale chest x-ray database and benchmarks on weakly-supervised classification and localization of common thorax diseases, in: *Proceedings of the IEEE conference on computer vision and pattern recognition*, 2017, pp. 2097–2106.
- [5] L. Nanni, A. Lumini, S. Brahnam, Local binary patterns variants as texture descriptors for medical image analysis, *Artificial intelligence in medicine* 49 (2) (2010) 117–125.
- [6] J. P. Cohen, P. Morrison, L. Dao, K. Roth, T. Q. Duong, M. Ghassemi, COVID-19 Image Data Collection: Prospective Predictions Are the Future, *arXiv preprint arXiv:2006.11988* (2020).
- [7] A. I. Khan, J. L. Shah, M. M. Bhat, Coronet: A deep neural network for detection and diagnosis of COVID-19 from chest x-ray images, *Computer Methods and Programs in Biomedicine* (2020) 105581.

- [8] T. Mahmud, M. A. Rahman, S. A. Fattah, CovXNet: A multi-dilation convolutional neural network for automatic COVID-19 and other pneumonia detection from chest X-ray images with transferable multi-receptive feature optimization, *Computers in Biology and Medicine* (2020) 103869.
- [9] L. Wang, A. Wong, COVID-Net: A Tailored Deep Convolutional Neural Network Design for Detection of COVID-19 Cases from Chest X-Ray Images, *arXiv preprint arXiv:2003.09871* (2020).
- [10] A. Z. Khuzani, M. Heidari, S. A. Shariati, COVID-Classifier: An automated machine learning model to assist in the diagnosis of COVID-19 infection in chest x-ray images, *medRxiv* (2020).
- [11] A. Krizhevsky, I. Sutskever, G. E. Hinton, Imagenet classification with deep convolutional neural networks, in: *Advances in neural information processing systems*, 2012, pp. 1097–1105.
- [12] K. Simonyan, A. Zisserman, Very deep convolutional networks for large-scale image recognition, *arXiv preprint arXiv:1409.1556* (2014).
- [13] C. Szegedy, W. Liu, Y. Jia, P. Sermanet, S. Reed, D. Anguelov, D. Erhan, V. Vanhoucke, A. Rabinovich, Going deeper with convolutions, in: *Proceedings of the IEEE conference on computer vision and pattern recognition*, 2015, pp. 1–9.
- [14] K. He, X. Zhang, S. Ren, J. Sun, Deep residual learning for image recognition, in: *Proceedings of the IEEE conference on computer vision and pattern recognition*, 2016, pp. 770–778.
- [15] A. Krizhevsky, G. Hinton, et al., Learning multiple layers of features from tiny images, *Tech. rep.*, Toronto (2009).
- [16] F. Chollet, Xception: Deep learning with depthwise separable convolutions, in: *Proceedings of the IEEE conference on computer vision and pattern recognition*, 2017, pp. 1251–1258.
- [17] S. Basu, S. Mitra, Deep Learning for Screening COVID-19 using Chest X-Ray Images, *arXiv preprint arXiv:2004.10507* (2020).
- [18] S. Rajaraman, J. Siegelman, P. O. Alderson, L. S. Folio, L. R. Folio, S. K. Antani, Iteratively Pruned Deep Learning Ensembles for COVID-19 Detection in Chest X-rays, *arXiv preprint arXiv:2004.08379* (2020).
- [19] G.-B. Huang, Q.-Y. Zhu, C.-K. Siew, Extreme learning machine: a new learning scheme of feedforward neural networks, in: *2004 IEEE international joint conference on neural networks (IEEE Cat. No. 04CH37541)*, Vol. 2, IEEE, 2004, pp. 985–990.
- [20] A. Akusok, K.-M. Björk, Y. Miche, A. Lendasse, High-performance extreme learning machines: a complete toolbox for big data applications, *IEEE Access* 3 (2015) 1011–1025.

- [21] S. Karpagachelvi, M. Arthanari, M. Sivakumar, Classification of electrocardiogram signals with support vector machines and extreme learning machine, *Neural Computing and Applications* 21 (6) (2012) 1331–1339.
- [22] J. Kim, H. S. Shin, K. Shin, M. Lee, Robust algorithm for arrhythmia classification in ECG using extreme learning machine, *Biomedical engineering online* 8 (1) (2009) 31.
- [23] J. Yang, S. Xie, S. Yoon, D. Park, Z. Fang, S. Yang, Fingerprint matching based on extreme learning machine, *Neural Computing and Applications* 22 (3-4) (2013) 435–445.
- [24] M. R. Daliri, A hybrid automatic system for the diagnosis of lung cancer based on genetic algorithm and fuzzy extreme learning machines, *Journal of medical systems* 36 (2) (2012) 1001–1005.
- [25] A. Rajpal, A. Mishra, R. Bala, A Novel fuzzy frame selection based watermarking scheme for MPEG-4 videos using Bi-directional extreme learning machine, *Applied Soft Computing* 74 (2019) 603–620.
- [26] A. Mishra, A. Rajpal, R. Bala, Bi-directional extreme learning machine for semi-blind watermarking of compressed images, *Journal of information security and applications* 38 (2018) 71–84.
- [27] R. Nian, B. He, A. Lendasse, 3D object recognition based on a geometrical topology model and extreme learning machine, *Neural Computing and Applications* 22 (3-4) (2013) 427–433.
- [28] J. A. Fill, D. E. Fishkind, The Moore–Penrose Generalized Inverse for Sums of Matrices, *SIAM Journal on Matrix Analysis and Applications* 21 (2) (2000) 629–635.
- [29] G.-B. Huang, Q.-Y. Zhu, C.-K. Siew, Extreme learning machine: theory and applications, *Neurocomputing* 70 (1-3) (2006) 489–501.
- [30] T. Rahman, M. Chowdhury, A. Khandakar, COVID-19 Radiography Database — Kaggle, <https://www.kaggle.com/tawsifurrahman/covid19-radiography-database> (2020).
- [31] D. Kermany, K. Zhang, M. Goldbaum, Large dataset of labeled optical coherence tomography (oct) and chest x-ray images, Mendeley Data, v3 [http://dx. doi. org/10.17632/rschjbr9sj](http://dx.doi.org/10.17632/rschjbr9sj) 3 (2018).
- [32] S. A. Ahmad, M. N. Taib, N. E. A. Khalid, H. Taib, An analysis of image enhancement techniques for dental X-ray image interpretation, *International Journal of Machine Learning and Computing* 2 (3) (2012) 292.
- [33] A. Jain, K. Nandakumar, A. Ross, Score normalization in multimodal biometric systems, *Pattern recognition* 38 (12) (2005) 2270–2285.
- [34] R. M. Haralick, K. Shanmugam, I. H. Dinstein, Textural features for image classification, *IEEE Transactions on systems, man, and cybernetics* 6 (1973) 610–621.

- [35] M. R. Zare, W. C. Seng, A. Mueen, Automatic classification of medical x-ray images, *Malaysian Journal of Computer Science* 26 (1) (2013) 9–22.
- [36] MathWorks, Texture Analysis Using the Gray-Level Co-Occurrence Matrix (GLCM) - MATLAB & Simulink, [https://www.mathworks.com/help/images/texture-analysis-using-the-gray-level-co-occurrence-matrix-glcm.html#:~:text=More-,Texture%20Analysis%20Using%20the%20Gray%20Level%20Co%20Occurrence%20Matrix%20\(,gray%20level%20spatial%20dependence%20matrix.](https://www.mathworks.com/help/images/texture-analysis-using-the-gray-level-co-occurrence-matrix-glcm.html#:~:text=More-,Texture%20Analysis%20Using%20the%20Gray%20Level%20Co%20Occurrence%20Matrix%20(,gray%20level%20spatial%20dependence%20matrix.) (2020).
- [37] N. Dalal, B. Triggs, Histograms of oriented gradients for human detection, in: 2005 IEEE computer society conference on computer vision and pattern recognition (CVPR'05), Vol. 1, IEEE, 2005, pp. 886–893.
- [38] GitHub, Histogram of Oriented Gradients, [https://scikit-image.org/docs/dev/auto\\_examples/features\\_detection/plot\\_hog.html](https://scikit-image.org/docs/dev/auto_examples/features_detection/plot_hog.html) (2020).
- [39] Z. Xue, D. You, S. Candemir, S. Jaeger, S. Antani, L. R. Long, G. R. Thoma, Chest x-ray image view classification, in: 2015 IEEE 28th International Symposium on Computer-Based Medical Systems, IEEE, 2015, pp. 66–71.
- [40] J. K. Kim, H. W. Park, Statistical textural features for detection of microcalcifications in digitized mammograms, *IEEE transactions on medical imaging* 18 (3) (1999) 231–238.
- [41] N. V. Shree, T. Kumar, Identification and classification of brain tumor MRI images with feature extraction using DWT and probabilistic neural network, *Brain informatics* 5 (1) (2018) 23–30.
- [42] J. M. Leibstein, A. L. Nel, Detecting tuberculosis in chest radiographs using image processing techniques, University of Johannesburg (2006).
- [43] N. Parveen, M. M. Sathik, Detection of pneumonia in chest X-ray images, *Journal of X-ray Science and Technology* 19 (4) (2011) 423–428.